Ab initio study of a charged vacancy in yttrium aluminum garnet ($Y_3Al_5O_{12}$)

2008 J. Phys.: Condens. Matter 20 325212

(http://iopscience.iop.org/0953-8984/20/32/325212)

J. Phys.: Condens. Matter **20** (2008) 325212 (6pp) doi:10.1088/0953-8984/20/32/325212

Ab initio study of a charged vacancy in yttrium aluminum garnet ($Y_3Al_5O_{12}$)

J Chen[1], T C Lu[2], Y Xu[1], A G Xu[1] and D Q Chen[1]

[1] Laboratory of Computational Physics, Institute of Applied Physics and Computational Mathematics, Beijing 100088, People's Republic of China
[2] Department of Physics, Sichuan University, Chengdu, Sichuan 610064, People's Republic of China

E-mail: jun_chen@iapcm.ac.cn

Received 29 January 2008, in final form 16 June 2008
Published 9 July 2008
Online at stacks.iop.org/JPhysCM/20/325212

Abstract

In this paper, various charged vacancies in yttrium aluminum garnet ($Y_3Al_5O_{12}$) are studied using the *ab initio* method. The local atomic structures, electronic structure, defect states, and formation energies of vacancies are calculated. The optical transition induced by an oxygen vacancy is predicted and the stability of the charged oxygen vacancy is discussed. Our results show that the 2+ charged oxygen vacancy is the easiest to form and is more stable than the other charged states of oxygen vacancies. A comparison between calculated and experimental results identifies that the absorption peak at 275 nm is attributed to the neutral oxygen vacancy, both the 300 and 580 nm peaks are induced by the 1+ charged oxygen vacancy.

(Some figures in this article are in colour only in the electronic version)

1. Introduction

Yttrium aluminum garnet ($Y_3Al_5O_{12}$, or YAG), as a very important solid-state laser host material [1–10], has been widely applied in the areas of medicine and industry. The optical properties of YAG with rare-earth dopants have been an important research area in order to improve the material processing and performance [1–9]. It has been recognized that point defects will be generated in the process of crystal growth and they will affect the optical and mechanical properties of the material [11–15]. For years, many experimental methods, including optical absorption [11–14], photoluminescence (PL) [12, 13], thermoluminescence (TL) [14, 15], etc, have been used to investigate the rare-earth doped and undoped YAG. Rich optical absorption and luminescence spectra have been obtained and some peaks in the spectrum have been attributed to the point defects in YAG, although the origin of defect-induced peaks has not been identified. For example, the absorption peaks at 300 nm [11], 225 nm, and 270 nm [12] have been attributed to be the host lattice defect in YAG. Recently, in a UV irradiated undoped YAG crystal, Wang *et al* [14] observed absorption peaks at 300 and 580 nm with a broad tail up to 750 nm. Their absorption peaks have been attributed to native defects or impurities in YAG. In the luminescence spectrum of Ce:YAG [13, 14], the 300 nm peak is also due to the host lattice defect.

On the other hand, theoretical calculations on YAG are very few [16–18]. This may be due to its complex crystal structure as discussed in section 2. The earliest calculations on the electronic structure of YAG and Cr-doped YAG were performed by Ching *et al* [17, 18] using the orthogonalized linear combination of atomic orbitals (OLCAO) methods. Kuklja [16] calculated the formation energies of Al, Y, and O vacancies in YAG by using the pair potential molecular dynamics method. Their calculated formation energies of point vacancies in YAG (Al(tet) 45.37 eV, Al(oct) 45.93 eV, Y 49.42 eV and O 21.54 eV) are larger than those of the Al or O vacancy in α-Al_2O_3 [20]. However, the electronic structure of the point vacancy in YAG has not been theoretically investigated up to now. The defect levels are therefore unknown, although optical properties of YAG crystals with defects have been extensively studied experimentally. The lack of reliable electronic structure information on defects makes the interpretation of the optical data difficult.

In this paper, we present results of the plane wave density functional theory (DFT) calculation of various point vacancies in crystal YAG. First-principle methods have been a powerful theoretical tool for acquiring accurate defect levels and optical properties of charged vacancies in metal oxides [19–25]. The present work attempts to theoretically characterize the point vacancy in YAG and to explain the experimental optical

Table 1. Defect formation energy (eV) and structural relaxation around each defect species. Average distances from the vacancy positions to neighboring atoms are listed. Neighboring atomic species and coordination numbers are also shown in parentheses. For perfect YAG, only the coordination number of the O atom is analyzed (cutoff distance is 4.5 Å).

		Averaged distance in Å (atomic species, coordination number)		
	Formation energy (eV)	1 NN	2 NN	3 NN
Perfect		1.75 (Al(tet), 1), 1.91 (Al(oct), 1), 2.34 (Y, 2)	3.10 (O, 14)	3.86 (Al, 8), 4.11 (Y, 4)
V_O^0	12.63 (21.54[a])	1.84 (Al(tet), 1), 2.02 (Al(oct), 1), 2.46 (Y, 2)	3.04 (O, 14)	3.86 (Al, 8), 4.11 (Y, 4)
V_O^{1-}	12.09	1.84 (Al(tet), 1), 2.03 (Al(oct), 1), 2.49 (Y, 2)	3.01 (O, 14)	3.87 (Al, 8), 4.12 (Y, 4)
V_O^{2-}	11.05	1.92 (Al(tet), 1), 2.21 (Al(oct), 1), 2.55 (Y, 2)	2.94 (O, 19)	3.87 (Al, 8), 4.13 (Y, 4)
$V^0_{Al(tec)}$	22.46 (45.37[a])	1.91 (O, 4)	3.43 (Al, 8), 3.35 (Y, 6)	3.72 (O, 18)
$V^0_{Al(oct)}$	22.69 (45.93[a])	2.11 (O, 6)	3.30 (Al, 6), 3.28 (Y, 6)	3.96 (O, 18)
V_Y^0	23.73 (49.42[a])	2.49 (O, 8)	3.30 (Al, 8), 3.57 (Y, 3)	4.05 (O, 14)

[a] Reference [16].

absorption spectrum. Our results will help to understand defects in YAG. This paper is organized as follows. In section 2 we describe the initial YAG model and the calculation method. In section 3 the calculated results are presented and discussed in detail. Section 4 summarizes and concludes the paper.

2. Model and method

The YAG crystal has a complicated garnet structure. It contains 80 (160) atoms in the primitive (cubic) cell [26], with a space group of O_h^{10}. The O atoms occupy the 96(h) sites. The Y ions occupy the 24(c) sites; each Y ion is dodecahedral coordinated to eight O atoms. There are two different sites for Al. The Al(oct) atoms occupy the 16(a) sites with an octahedral point symmetry, and the Al(tet) atoms occupy the 24(d) sites with a tetrahedral point symmetry. In the present work, we use the 160-atom cubic cell as our initial YAG model (see figure 1). It is big enough for studying the effect of vacancy. We relax the cell volume and atomic positions of the initial YAG model by using the Vienna *Ab initio* Simulation Package (VASP) [27]. The optimal lattice constant of our YAG model is 11.84 Å which has a 1.33% error compared with the experimental value of 12.0 Å [26]. The relaxed bond lengths of Y–O and Al–O are listed in table 1. For our initial YAG system, the Y–O bond lengths are 2.29 and 2.38 Å; the bond length of Al(tet)–O is 1.91 Å and that of Al(oct)–O is 1.75 Å.

The neutral oxygen vacancy V_O^0 is created by removing one oxygen atom from the initial YAG system. The 1+ charged oxygen vacancy V_O^{1+} or 2+ charged oxygen vacancy V_O^{2+} is created by removing one electron or two electrons from the neutral V_O^0 system, respectively. For completeness, we also create the neutral Y or Al vacancy in the same way as the neutral O vacancy. They are denoted by $V_Y^0 V^0_{Al(tec)}$ and $V^0_{Al(oct)}$, respectively.

All calculations were carried out using VASP [27], implementing the generalized gradient approximation (GGA) of Perdew–Wang 91 (PW-91). We used a plane wave basis set with an energy cutoff of 400 eV and eight k points in the irreducible wedge of the Brillouin zone (IBZ). The total energy attains an accuracy of at least 0.001 eV and

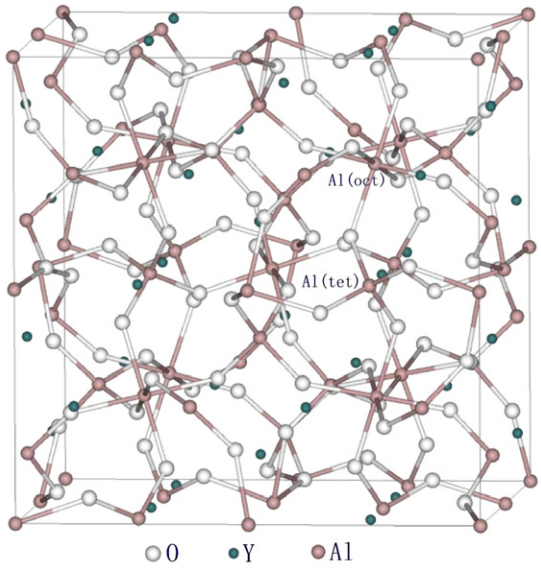

Figure 1. The initial model of perfect crystalline YAG. It contains 160 atoms in total. One octahedral Al atom and one tetrahedral Al atom are indicated. Every Y atom is at same dodecahedron site and has eightfold bonds. All Y–O bonds are eliminated in this diagram in order to show the Al–O bond well.

the residual force converges to about 0.01 eV $Å^{-1}$. All charged defect calculations were performed by following the standard procedures [27] of imposing a neutralizing uniform background charge followed by monopole–dipole–quadrupole corrections with the low-frequency dielectric constant of $\varepsilon = 11.7$. Then, we need to mention that the total energies of charged defect systems are calculated based on the neutral cell by VASP.

The charged O vacancy formation energy $E_{for}(vac, q)$ is calculated according to [19]

$$E_{for}(vac, q) = E(vac, q) - E(per) + E(O, q), \qquad (1)$$

where $E(vac, q)$, $E(per)$, and $E(O, q)$ are the energies of the relaxed vacancy model, of the perfect YAG model, and of an isolated oxygen ion, respectively. Here, $E(O, q)$ is calculated

by using a cell with the same size as that of the vacancy model but containing only one oxygen atom with charge q. Here, we need to mention that, $E(\mathrm{O}, q)$ should be the energy of a single oxygen ion at the fourfold coordination state but not of the isolated oxygen ion. Yet, it is difficult to calculate the energy of a single oxygen ion at the fourfold coordination state in the first-principle methods. Our approach may lead to the slightly overestimated formation energy. The formation energy of the Al or Y vacancy can be obtained in the same way.

The stability of a charge state of a vacancy is determined by the position of the vacancy-induced defect levels with respect to the local chemical potential. For vacancies close to the metal–insulator interface, the local chemical potential is largely determined by the metal Fermi level. The Fermi energy (E_F) is defined with respect to the valence band minimum of vacancy systems. Hence, the stability of charged vacancy systems compared to their neutral counterparts is determined by the relative total energy $E_\mathrm{rel}(\mathrm{vac}, q)$ as a function of E_F [22],

$$E_\mathrm{rel}(\mathrm{vac}, q) = E(\mathrm{vac}, q) + q(E_\mathrm{F} - E_\mathrm{V}) - E(\mathrm{vac}, 0) + k. \quad (2)$$

Here k is the relative correction for the DFT underestimation of the band gap (E_g), which equals the difference between the theoretical E_g and the experimental E_g. E_V is the top edge of the valence band. $E(\mathrm{vac}, q)$ and $E(\mathrm{vac}, 0)$ are defined as above.

3. Results and discussion

3.1. Relaxed structure and formation energy

Firstly, we relax all models of YAG with various vacancies. The existence of a vacancy induces distortion of the local geometry around the defect. The distances between vacancies and surrounding atoms after relaxation are examined and summarized in table 1. It is noted that atoms in a certain coordination shell do not always have the same distance from a vacancy, which is due to the low symmetry of the YAG crystal. In the case of V_O^0, the second-nearest neighboring (2NN) eight O ions move closer to the vacancy by 2%–3% of their original distances. While for first-nearest neighboring (1NN) four cations, two Y, one Al(tet), and one Al(oct), all move away from the oxygen vacancy. But, different cations have different behaviors. The two Y ions move away by about 0.12 Å and the Al(oct) ion moves away by about 0.11 Å. The distance moved by the Al(tet) ion is the shortest at 0.09 Å. This can be understood in terms of the electrons localized to the vacancy site. The creation of a neutral oxygen vacancy leaves behind two electrons localized to the vacancy site. So, in comparison with the original interaction between the oxygen and surrounding ions, there are only weak electrostatic attractions or repulsions between a vacancy and its surrounding ions, which explains the distortion of the ions.

The situation for $\mathrm{V}_\mathrm{O}^{1+}$ or $\mathrm{V}_\mathrm{O}^{2+}$ is similar to that of V_O^0. The $\mathrm{V}_\mathrm{O}^{1+}$ behaves like a positively charged vacancy with one electron, whereas the $\mathrm{V}_\mathrm{O}^{2+}$ behaves like a double positively charged vacancy. Because of the weaker electrostatic interaction between a vacancy and its surrounding ions compared with the case of V_O^0, the ionic displacement away from a vacancy in these two cases is larger. The nearest two Y and two Al ions surrounding the vacancy are again accompanied by further displacement away from the vacancy site by an additional 0.01–0.03 Å for $\mathrm{V}_\mathrm{O}^{1+}$ and 0.08–0.09 Å for $\mathrm{V}_\mathrm{O}^{2+}$.

In the case of the neutral V_Y^0, the 1NN eight oxygen ions surrounding the Y vacancy are displaced outwards by about 0.15 Å, and for the case of the neutral $\mathrm{V}_\mathrm{Al(tet)}$ ($\mathrm{V}_\mathrm{Al(oct)}^0$), the 1NN six oxygen ions (four oxygen ions) are displaced by about 0.17 Å (0.20 Å) from the Al vacancy. We also note that the local ionic distortion in the case of the neutral cation vacancy is significantly stronger than that of the neutral oxygen vacancy.

Based on the calculated total energies of the relaxed vacancy systems, the formation energies of various vacancy species are evaluated and listed in table 1. The theoretical values from the molecular dynamics (MD) method by Kuklja *et al* [16] are also listed for comparison. One can see that the MD formation energies of neutral O, Al, and Y vacancies are higher than our results by a factor of 2. This may be attributed to the potential parameters used in MD calculations. We did not find any experimental results to compare with. However, we note that our formation energy of a neutral O vacancy (12.63 eV) is close to that of an O vacancy in α-$\mathrm{Al_2O_3}$ (13.50 eV) [20] and in MgO (8.90 eV) [28]. For various cases with O vacancies, the $\mathrm{V}_\mathrm{O}^{2+}$ exhibits the smallest formation energy. It means that $\mathrm{V}_\mathrm{O}^{2+}$ is the easiest species to form among the three investigated cases with an O vacancy. For the case of a cation vacancy, the V_Y^0 has a larger formation energy than the $\mathrm{V}_\mathrm{Al(tet)0}$ and than $\mathrm{V}_\mathrm{Al(oct)0}$. This can be understood as follows. The Y ion is at the dodecahedron site and has eightfold bonds, while the Al(tet) has only fourfold bonds and the Al(oct) has sixfold bonds. So, removing a Y ion needs more energy than removing an Al ion.

3.2. Electronic structure and optical transition

In order to locate the defect energy levels induced by a vacancy, we calculate the electronic density of states (DOS) and partial DOS (PDOS) of YAG with and without a vacancy. The DOS of a perfect YAG model is plotted in figure 3(a). The total characters are as follows: the O-2s levels are between −18.0 and −16.5 eV and the O-2p levels constitute the upper valence band (VB) with a total width of about 6.5 eV. The Y-3d, 4s and Al-2p, 3s constitute the conduction band (CB) and at the bottom of the CB, Y-3d has the largest component. All characters are similar to the calculated DOS using the OLCAO method [17]. Our calculated band gap E_g is 4.50 eV, which is very close to the value of 4.3 eV [17] by the OLCAO method, but it is smaller than the experimental values of 6.5–7.0 eV [29, 30]. Such a discrepancy is expected when the DFT method is used. In the calculation for optical transition energy and in the relative stability analysis of defect states, all defect energy in the gap will be shifted by $k = 2.0$ eV as mentioned above in formula (2).

As can be seen from figures 2(b)–(g), the overall DOS profiles of various defect systems are quite similar to that of a perfect YAG. However, The new defect energy levels are

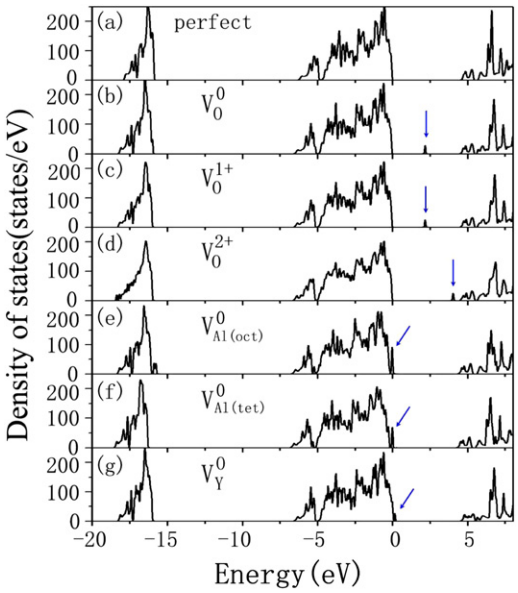

Figure 2. Calculated density of states for YAG with and without vacancies. The valence band maxima are set at 0 eV. The defect energy levels are denoted by arrows. (a) Perfect YAG; (b) YAG + V_O^0; (c) YAG + V_O^{1+}; (d) YAG + V_O^{2+}; (e) YAG + $V_{Al(oct)}^0$; (f) YAG + $V_{Al(tet)}^0$; (g) YAG + V_Y^0;

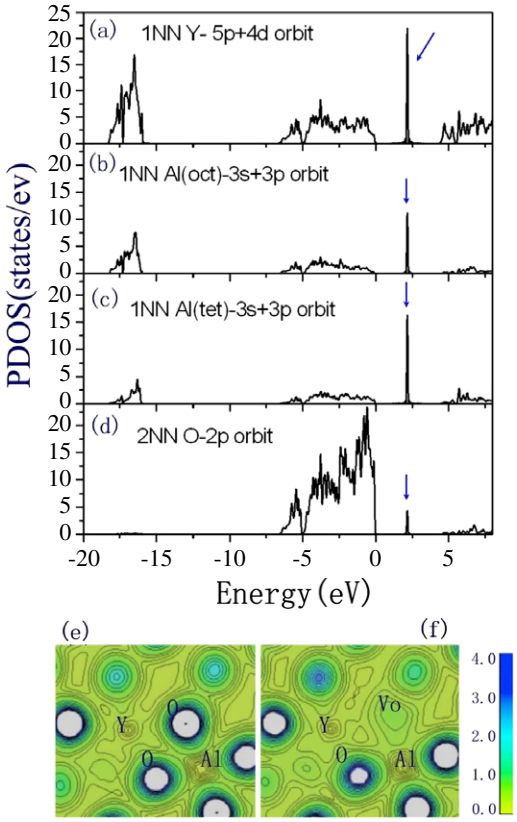

Figure 3. Calculated partial density of states of an ion adjacent to an O vacancy and the charge contour map of the neutral V_O^0: (a) PDOS of Y-5p + 4d orbits; (b) PDOS of Al(oct)-3s + 3p orbits; (c) PDOS of Al(tet)-3s + 3p orbits; (d) PDOS of O-2p orbit; (e) the charge contour of a perfect YAG (in the units of electron/cell volume); (f) the charge contour of YAG + V_O^0.

induced around the VB or CB edges. In the case of V_O^0 (figure 2(b)), a two-electron occupied level at 2.2 eV above the VB edge is introduced. The V_O^{1+} (figure 2(c)) induces a one-electron occupied defect level at 2.3 eV above the VB edge, but the vacancy V_O^{2+} (figure 2(d)) displays a shallow unoccupied state 0.5 eV below the CB. In contrast, the defect states of all cation vacancies are located at the edge of the VB and all are unoccupied, as marked by the arrows in figures 2(e)–(g). Hence, all cation vacancies introduce acceptor-like states above the VB.

In order to investigate the features of defect states in the vacancy system, we choose to analyze PDOS of the neutral case V_O^0. The PDOS of 1NN Y and Al ions, and 2NN O ion are shown in figures 3(a)–(d). The defect state at 2.2 eV above the VB is mainly composed of the 1NN Al-3s + 3p orbitals, the 1NN Y-5p + 4d orbitals, and the partial 2NN O-2p orbital. As shown in figure 3(f), there is a strongly localized charge distribution close to the site of the oxygen vacancy. Comparing the above PDOS analysis, this charge localization is due to the Al-3s, 3p orbitals, the Y-5p, 4d orbitals, and the partial O-2p orbital extending to the area of the vacancy. Although the Al-3s, 3p and the Y-5p, 4d orbitals constitute the CB in perfect YAG, such localization of the Al-3s, 3p and the Y-4d, 5p orbitals will shift the energy level downward from the CB edge, resulting in the formation of a deep defect level in the middle of the band gap. Our analysis also shows that the defect states of V_Y^0, $V_{Al(tet)0}$ and $V_{Al(oct)0}$ are mainly constituted by the adjacent O-2p orbital. Therefore, defect states of cation vacancies are located at the top of the VB, as shown in figures 2(e)–(g).

The optical absorption spectrum is important for studying defects in YAG. The above-mentioned defect states will lead to new optical absorption. Considering the influence of the final-relaxation effect, ground state eigenvalues by the DFT generally do not represent well the one-electron binding energies. In the present work, the vertical transition energies of defect states are calculated based on the total energy of charged vacancy systems [19, 22]. This approach has been proved to be highly accurate.

Here we set four optical transition models for various charged oxygen vacancies, as shown in figure 4. Model I is an electron transition from the defect state of the V_O^0 to the CB, where the calculated excitation energy is 4.60 eV. This can be written as V_O^0 + phonon $\rightarrow$ V_O^{1+} + e. Model II is an electron transition from the defect level of the V_O^{1+} to the CB, where the excitation energy is 4.22 eV. This process is represented as V_O^{1+} + phonon $\rightarrow$ V_O^{2+} + e. Model III is an electron transition from the top of the VB to the defect state of V_O^{1+}, where the excitation energy is 2.34 eV. This is written as V_O^{1+} + e + phonon $\rightarrow$ V_O^0. Model IV is an electron transition from the top of the VB to the shallow unoccupied level of V_O^{2+}, where the excitation energy is 6.11 eV. This can be written as V_O^{2+} + e + phonon $\rightarrow$ V_O^{1+}.

Our calculated excitation energies agree well with the experimental values. In the irradiated undoped YAG sample, peaks at 300 nm (4.11 eV) [11, 14], 270 nm (4.57 eV) [12], and 580 nm (2.13 eV) [14] have been found in the optical

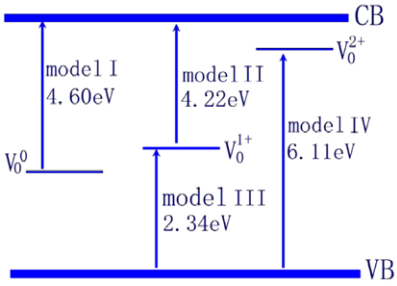

Figure 4. Predicted optical transition models induced by neutral and charged oxygen vacancies in YAG.

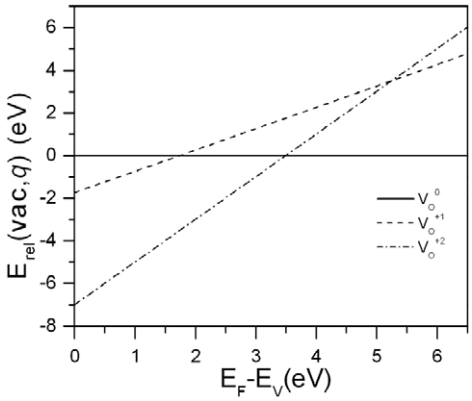

Figure 5. Relative total energy $E_{\rm rel}(\mathrm{vac}, q)$ of a charged O vacancy as a function of local Fermi energy, where q denotes the charge state of the O vacancy ($q = 0, +1, +2$).

absorption spectrum. Compared with our defect optical transition models, the 270 nm (4.57 eV) [12] peak is attributed to V_{O0}, (see model I, 4.60 eV), where there is an electron transfers from the V_O^0 state to the CB. The 300 nm (4.11 eV) peak corresponds to the excitation energy of 4.22 eV of model II where an electron transfers from the V_O^{1+} state to the CB. The 580 nm (2.13 eV) peak [14] is consistent with the excitation energy of 2.34 eV of model III. Then, the 580 nm peak is attributed to the electron transition from the VB to the V_O^{1+} state. As for model IV, where an electron transfers from the VB to V_{O2+} state, we have no experimental results to compare. As its excitation energy (6.11 eV) is close to the experimental band gap 6.5 eV, the absorption peak of model IV should be close to the edge of the intrinsic absorption of YAG. In [14], Wong *et al* observed a broad absorption spectrum where there are two peaks at 300 and 580 nm with a long tail up to 750 nm in the UV irradiated undoped YAG sample. This broad spectrum could not be assigned to a single defect, instead, it must be a cooperative effect of different deep energy level defects. Our models II and III can explain the peaks at 300 and 580 nm, but, to interpret the broad tail, more calculations on other defect species in YAG are necessary.

3.3. Relative stability of charged oxygen vacancy

Finally, we examine which is the most stable defect species of neutral and charged oxygen vacancies based on the obtained system total energies. The relative total energies $E_{\rm rel}(\mathrm{vac}, q)$ of various charged oxygen vacancies are plotted as a function of $(E_{\rm F} - E_{\rm V})$ in figure 5. Considering figure 5, for a wide range of $E_{\rm F} - E_{\rm V}$ (<3.5 eV), the V_O^{2+} is predicted to be most stable, and for high values of $E_{\rm F} - E_{\rm V}$, the neutral V_O^0 is seen to be most stable. These predictions are consistent with the location of the occupied state at the mid gap, and the unoccupied state close to the conduction band in the case of oxygen vacancies. Clearly, when $E_{\rm F} - E_{\rm V}$ is low, the two electrons from the occupied state will tend to be transferred to the Fermi level, making the V_O^0 and V_O^{1+} state not stable, and the V_{O2+} state more stable, while no transfer of charge will occur for other values of $E_{\rm F} - E_{\rm V}$, making the neutral state most stable. Thus, with the exception of the small $E_{\rm F} - E_V$ ranges at which the neutral V_O^0 charge state is stable, the V_{O2+} state is seen to be most stable for a wide range of $E_{\rm F} - E_{\rm V}$.

4. Summary

In this paper, *ab initio* pseudopotential calculations have been performed to study the properties of charged vacancies in YAG. The electronic structure, formation energy, defect states, and relative stability of various charged vacancies have been investigated. Our results can be summarized as follows.

(1) A charged vacancy introduced new defect states in the band gap. For the oxygen vacancy, the neutral V_O^0 and charged V_O^{1+} induced deep defect levels at the middle of the band gap and V_O^{2+} induced a shallow level near the bottom of the CB. For the cation vacancies (Y, Al(tet), Al(oct)), all the defect levels are located at the edge of the VB.

(2) After comparing our predicted transition models with the optical absorption spectra, we assign the absorption peak 275 nm to V_O^0, and the 300 nm and 580 nm peaks both to V_O^{1+} by electron transitions from the defect state to the CB or from the VB to the defect state, respectively.

(3) Lastly, our results show that the V_O^{2+} state forms oxygen vacancy species most easily and also is the most stable of all three charged oxygen vacancies in a wide range of $E_{\rm F} - E_{\rm V}$.

Acknowledgments

This work was supported by the National Nature Science Foundation of China (grant Nos. 10744002 and 10774017). This research used the resources of Shenteng-6800 supported by SCCAS.

References

[1] Lee S, Choi D, Kim C-J and Zhou J 2007 Highly efficient diode side-pumped Nd:YAG ceramic laser with 210 W output power *Opt. Laser Technol.* **39** 705

[2] Trofimor A, Petrova M and Zamoryanskaya M 2007 Cathodoluminescence properties of yttrium aluminum garnet doped with Eu^{+2} and Eu^{+3} ions *Semiconductors* **41** 512

[3] Owen J F, Dorain P B and Kobayosi T 1981 Excited-state absorption in Eu^{2+}:CaF_2 and Ce^{3+}:YAG single crystals at 298 and 77 K *J. Appl. Phys.* **52** 1216
[4] Van der Weg W F and Van Tol M W 1981 Saturation effects of cathodoluminescence in rare-earth activated epitaxial $Y_3Al_5O_{12}$ layers *Appl. Phys. Lett.* **38** 705
[5] Liu Q, Gong M, Lu F, Gong W and Li C 2005 520-W continuous-wave diode corner-pumped composite Yb:YAG slab laser *Opt. Lett.* **30** 726
[6] Zhang H, Han H, Su C, Zhang H, Hou Z and Song Q 2007 Application of stereology on microstructure of neodymium-doped yttrium aluminum garnet (Nd:YAG) transparent ceramics *Mater. Sci. Eng.* A **445** 180
[7] Ikesue A, Yoshida K and Kamata K 1995 Fabrication and optical properties of high-performance polycrystalline Nd:YAG ceramics for solid-state lasers *J. Am. Ceram. Soc.* **78** 1033
[8] Ikesue A, Yoshida K and Yamamoto T 1997 Optical scattering centers in polycrystalline Nd:YAG laser *J. Am. Ceram. Soc.* **80** 1517
[9] Pastor J Y, Llorca J and Salazar A 2005 Mechanical properties of melt-grown alumina–yttrium aluminum garnet eutectics up to 1900 K *J. Am. Ceram. Soc.* **88** 1488
[10] Cinibulk M K, Parthasarathy T A, Keller K A and Mah T-I 2002 Porous yttrium aluminum garnet fiber coatings for oxide composites *J. Am. Ceram. Soc.* **85** 2703
[11] Bagdasarov Kh S, Pasternak L B and Sevast'yanov B K 1977 Dependences of the absorption and luminescence spectra of $Y_3Al_5O_{12}$: Cr^{3+} crystals on chromium concentration *Sov. J. Quantum Electron.* **7** 965
[12] Wong C M, Rotman S R and Warde C 1984 Optical studies of cerium doped yttrium aluminum garnet single crystals *Appl. Phys. Lett.* **44** 1038
[13] Robbins D J, Cockayne B, Lent B, Duckworth C N and Glasper J L 1979 Investigation of competitive recombination processes in rare-earth activated garnet phosphors *Phys. Rev.* B **19** 1254
[14] Wang C L, Solodovnikov D and Lynn K G 2006 Point defects in Ce-doped $Y_3Al_5O_{12}$ crystal scintillators *Phys. Rev.* B **73** 233204
[15] Xu X, Zhao Z, Song P, Zhou G, Xu J and Deng P 2004 Structureal, thermal, and luminescent properties of Yb-doped $Y_3Al_5O_{12}$ crystals *J. Opt. Soc. Am.* B **21** 543
[16] Kuklja Maija M 2000 Defects in yttrium aluminium perovskite and garnet crystals:atomistic study *J. Phys.: Condens. Matter* **12** 2953
[17] Xu Y N and Ching W Y 1999 Electronic structure of yttrium aluminum garnet ($Y_3Al_5O_{12}$) *Phys. Rev.* B **59** 10530
[18] Ching W Y, Xu Y N and Brickeen B K 1999 *Ab initio* calculation of excited state absorption of Cr^{4+} in $Y_3Al_5O_{12}$ *Appl. Phys. Lett.* **74** 3755
[19] Foster A S, Sulimov V B, Gejo F L, Shluger A L and Nieminen R M 2001 Structure and electrical levels of point defects in monoclinic zircinia *Phys. Rev.* B **64** 224108
[20] Matsunaga K, Tanaka T, Yamamoto T and Ikuhara Y 2003 First-principles calculations of intrinsic defects in Al_2O_3 *Phys. Rev.* B **68** 85110
[21] Lany S and Zunger A 2004 Metal-dimer atomic reconstruction leading to deep donor states of the anion vacancy in II–VI and chalcopyrite semiconductors *Phys. Rev. Lett.* **93** 156404
[22] Ramprasas R 2003 First principle study of oxygen vacancy defects in tantalum pentoxide *J. Appl. Phys.* **94** 5609
[23] Jiang Y, Adams J B and Schilfgaarde M V 2005 Theoretical study of environmental dependence of oxygen vacancy formation in CeO_2 *Appl. Phys. Lett.* **87** 141917
[24] Yokozawa A and Miyamoto Y 1997 First principles calculations for charged states of hydrogen atoms in SiO_2 *Phys. Rev.* B **55** 13783
[25] Chen J, Rulis P, Ouyang L, Satpathy S and Ching W Y 2006 Vacancy-enhanced ferromagnetism in Fe-doped rutile TiO_2 *Phys. Rev.* B **74** 235207
[26] Euler F and Bruce J A 1965 Oxygen coordinates of compounds with garnet structure *Acta Crystallogr.* **19** 971
[27] Kress G and Furthmuller J 1996 Efficient iterative schemes for *ab initio* total-energy calculations using a plane-wave basis set *Phys. Rev.* B **54** 11169
[28] Sulimov V, Casassa S, Pisani C, Garapon J and Poumellec B 2000 Embedded cluster *ab initio* study of the neutral oxygen vacancy in quartz and cristobalite *Modelling Simul. Mater. Sci. Eng.* **8** 763
[29] Thiel C W, Cruguel H, Wu H, Sun Y, Lapeyre G J, Cone R L, Equall R W and Macfarlane R M 2001 Systematics of 4f electron energies relative to host bands by resonant photoemission of rare-earth ions in aluminum garnets *Phys. Rev.* B **64** 085107
[30] Zych E, Brecher C and Glodo J 2000 Kinetics of cerium emission in YAG:Ce single crystal: the role of traps *J. Phys.: Condens. Matter* **12** 1947